1-1-2001

Molecular simulations of sound wave propagation in simple gases

Alejandro Garcia
San Jose State University, alejandro.garcia@sjsu.edu

N. Hadjiconstantinou
Massachusetts Institute of Technology

Recommended Citation

Alejandro Garcia and N. Hadjiconstantinou. "Molecular simulations of sound wave propagation in simple gases" *Physics of Fluids* (2001): 1040-1046. https://doi.org/http://dx.doi.org/10.1063/1.1352630

Molecular simulations of sound wave propagation in simple gases

Nicolas G. Hadjiconstantinou
Mechanical Engineering Department, Massachusetts Institute of Technology, Cambridge, Massachusetts 02139

Alejandro L. Garcia[a)]
Center for Applied Scientific Computing, Lawrence Livermore National Laboratory, Livermore, California 94551

(Received 25 July 2000; accepted 11 January 2001)

Molecular simulations of sound waves propagating in a dilute hard sphere gas have been performed using the direct simulation Monte Carlo method. A wide range of frequencies is investigated, including very high frequencies for which the period is much shorter than the mean collision time. The simulation results are compared to experimental data and approximate solutions of the Boltzmann equation. It is shown that free molecular flow is important at distances smaller than one mean free path from the excitation point. © *2001 American Institute of Physics.*
[DOI: 10.1063/1.1352630]

I. INTRODUCTION

In this article we study the propagation of high frequency sound waves in a dilute gas using the direct simulation Monte Carlo (DSMC) technique. Our investigation focuses on the variation of the wave speed and absorption coefficient as a function of frequency, ω. When the period of oscillation is comparable to the molecular collision time, the sound speed is known to deviate from the classical adiabatic constant. Similarly, at high frequencies the attenuation rate deviates significantly from the classical behavior observed in the low attenuation limit.[1,2]

Cercignani[3] surveys the various molecular kinetic formulations based on the Boltzmann equation that attempt to capture this phenomenon. These theories predict that at high frequencies the sound speed increases with frequency and that the absorption coefficient, which in the classical theory increases proportionally to the square of the frequency, exhibits a shallow maximum. Agreement with experimental data[4,5] over a frequency range that spans five orders of magnitude varies from moderate to good depending on the model. Surprisingly, the Maxwell molecule assumption, which simplifies the solutions significantly, seems to yield the same overall level of agreement with experimental data as the hard sphere approximation that is more appropriate for simple gases. Among the theoretical approaches discussed in Ref. 3, the 11-moment method of Sirovich and Thurber[6] is, in general, in best agreement with the experimental data.

We have performed accurate numerical calculations to obtain the wave speed and attenuation coefficient using the direct simulation Monte Carlo (DSMC) method. These results are a useful complement to the experimental data available, especially since the latter are subject to significant scatter in the high frequency range. Comparison of our results with analytical solutions can assess the validity of approximations involved in the latter; comparison of our results with experimental data evaluates the ability of the Boltzmann equation as a mathematical model to capture the physical reality observed in the experiments. DSMC offers considerable flexibility with respect to molecular interaction models that can be used; the present study uses the hard-sphere model that is typically assumed in the development of theory. Further refinements that will improve the connection and direct comparison to experimental data are discussed in the last section of the article.

Our calculations confirm that the predictions of the Navier–Stokes, Burnett and super-Burnett theories are only qualitatively correct. Good agreement is found between our results and the work of Sirovich and Thurber for hard sphere gases. Agreement with experiments is equally good. The effect of free molecular flow close to the excitation point is also elucidated through our calculations.

II. WAVE PROPAGATION USING DSMC: NUMERICAL TECHNIQUE

Figure 1 shows a sketch of the simulation geometry, a rectangular domain of length L filled with a dilute gas. Standard DSMC[7,8] techniques were used to simulate the gas since it is well established that DSMC accurately models high Knudsen number flows in which the characteristic length scale (in our case the acoustic wavelength, l) is comparable to the mean free path, λ. For the sake of brevity we will not present a description of the DSMC algorithm. Excellent introductory[7] and detailed[8] descriptions of DSMC, as well as formal derivations,[9] can be found in the literature. Comparisons of DSMC simulation results with solutions of the linearized Boltzmann equation and experimental results for diverse nonequilibrium phenomena spanning the whole Knudsen range can be found in Ref. 8 and 10.

In our simulations sound waves are excited at $x=0$ by imposing a sinusoidally varying velocity in the x-direction. The velocity is imposed using the well-known Maxwellian

[a)]Permanent address: Department of Physics, San Jose State University, San Jose, CA 95192-0106. Electronic mail:ngh@mit.edu

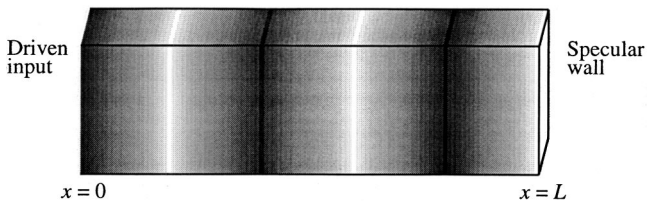

FIG. 1. Simulation geometry.

reservoir method: particles exiting the domain at $x=0$ are discarded, whereas particle influx is accounted for by a reservoir attached to the simulation domain at $x=0$ and extending to $x=-L_R$. Each timestep, particles at the simulation mean density are generated inside the reservoir and are given velocities drawn from a Maxwellian distribution at the simulation temperature. The Maxwellian distribution has a time-dependent mean velocity in the x-direction that is equal to the desired ''boundary condition.'' The particle positions are advanced in time (one timestep Δt); the particles that cross the imaginary plane $x=0$ and enter the simulation domain represent the half-space Maxwellian influx and are retained. The particles remaining in the reservoir are discarded and the simulation proceeds as usual. The length of the reservoir is set to $L_R=v_{\text{cutoff}}\Delta t$, where v_{cutoff} is a velocity for which the probability (based on a Maxwellian distribution) is very small. In the simulations we take $v_{\text{cutoff}}=6\sqrt{2k_BT/m_m}$ where k_B is Boltzmann's constant, T is the temperature, and m_m is the molecular mass.

In order to minimize the cost of our simulations the domain length L was taken to be no longer than a few wavelengths. The far end of the domain was terminated by a specular wall leading to total reflection of the propagating waves. In the absence of dissipation, the system would exhibit pure standing waves. At low frequencies attenuation is relatively small and the reflected wave is only slightly diminished with respect to the incoming wave. At higher frequencies no appreciable reflected wave exists.

The simulation geometry resembles that of the acoustic interferometer used in the experiments in Ref. 11 but with three differences. First, the acoustic source is a reservoir rather than a transducer: the reservoir generates a Maxwellian influx distribution which approximates that produced by a thermal wall, which in turn approximates the transducer used in the experiments; the reservoir, however, does not model the change in position of the wall. The second difference is that experimental measurements are taken at only a few output receivers whereas in the simulations the velocity variation, $v(x,t)$, is computed everywhere. This permits us to obtain the sound speed and attenuation coefficient without interferometry, i.e., without having to vary the domain length. Third, and perhaps most importantly, our evaluation of the velocity field is nonintrusive, in contrast to the receivers used in the experiments.

Waves propagating in the x direction lead to a velocity variation $v_o\exp\{i(\omega t-kx)-mx\}$ where $k=2\pi/l$ is the wavenumber, and m is the attenuation coefficient. The wave amplitude used was small to avoid nonlinear effects. Specifically, the viscous terms dominate the nonlinear terms when $v_o\ll\omega\mu/\rho c$ where μ is the viscosity, ρ is the mass density and c is the classical sound speed.[12] It will be convenient to express this criterion as $v_o\ll c/\mathrm{R}$ where $\mathrm{R}=c^2\rho/\omega\mu$ is the acoustic Reynolds number.

In the case of high frequency waves ($\mathrm{R}<0.5$) larger initial amplitudes were used (up to $v_o=0.15c$) because the attenuation is large and the amplitude damped considerably (see Sec. IV). At intermediate frequencies ($0.5\leqslant\mathrm{R}\leqslant4$) the amplitude was $v_o=0.05c$, whereas at the lowest frequencies ($\mathrm{R}>4$) the amplitude was $v_o=0.025c$; the above criterion ($v_o\ll c/\mathrm{R}$) is thus not satisfied for $\mathrm{R}>20$. However, the distance that a wave must travel before it significantly steepens due to nonlinear effects[12] is $L_{\text{nl}}=cl/\pi(\gamma+1)v_o$, where γ is the ratio of heat capacities ($\gamma=\frac{5}{3}$ for the monatomic gas studied here). The systems we consider are small ($L=\frac{7}{4}l$) so $L_{\text{nl}}\geqslant2.7L$. From these arguments we expect the effects of nonlinearities to be small at both the high and low frequency ranges. Additionally, simulations with the following wave amplitudes were performed: $v_o=0.05c$, $0.0125c$ at $\mathrm{R}=40$, $v_o=0.0125c$, $0.00625c$ at $\mathrm{R}=80$, and $v_o=0.05c$, $0.0125c$, $0.00625c$, $0.003125c$ at $\mathrm{R}=120$; these confirmed that nonlinear effects were small and did not affect our estimation of m and k.

The reflected wave is of the form $v_o\exp\{i(\omega t+kx)-m(2L-x)\}$. Superposition leads to a standing wave of the form

$$\begin{aligned}v(x,t)&=v_o[(e^{-mx}+e^{-m(2L-x)})\cos kx\sin\omega t\\&\quad-(e^{-mx}-e^{-m(2L-x)})\sin kx\cos\omega t]\\&=A(x)\sin\omega t+B(x)\cos\omega t.\end{aligned}\tag{1}$$

After the initial transients have passed, the velocity field is evaluated at each timestep in slices perpendicular to the x-axis. The chi-square fit to this data gives[13]

$$A(x_j)=\frac{\Sigma s^2\Sigma vc-\Sigma sc\Sigma vs}{\Sigma c^2\Sigma s^2-(\Sigma sc)^2},\tag{2}$$

$$B(x_j)=\frac{\Sigma c^2\Sigma vs-\Sigma sc\Sigma vc}{\Sigma c^2\Sigma s^2-(\Sigma sc)^2},\tag{3}$$

where

$$\Sigma s^2=\sum_i^M\sin^2\omega t_i,\quad \Sigma c^2=\sum_i^M\cos^2\omega t_i,$$

$$\Sigma sc=\sum_i^M\sin\omega t_i\cos\omega t_i,\quad \Sigma vs=\sum_i^M v(x_j,t_i)\sin\omega t_i,$$

$$\Sigma vc=\sum_i^M v(x_j,t_i)\cos\omega t_i,$$

with x_j being the position of the slice and M being the number of time samples recorded. The Nelder–Mead simplex method[13] is used to perform a nonlinear chi-square fit of $A(x)$ and $B(x)$ to extract the wavenumber k and the attenuation coefficient m. At the lowest frequencies ($\mathrm{R}>10$), $B(x)\ll A(x)$ and so the estimation of m and k was based on $A(x)$, or $\sqrt{A(x)^2+B(x)^2}$. Due to entrance effects, at the

higher frequencies ($R<0.5$) a phase shift is also included in the parameter fits. Entrance effects are further discussed in Sec. IV.

III. THEORIES FOR WAVE PROPAGATION IN HOMOGENEOUS MEDIA

The classical Navier–Stokes theory is limited to low frequencies (attenuations) and predicts a constant sound speed $c=\sqrt{\gamma k_B T/m_m}$, and an attenuation coefficient that is proportional to the square of the frequency[2]

$$m=\frac{\omega^2}{2\rho c^3}\left[\left(\frac{4}{3}\mu+\zeta\right)+\frac{\kappa}{c_p}(\gamma-1)\right]. \tag{4}$$

Here ζ is the coefficient of bulk viscosity, κ is the coefficient of thermal conductivity, and c_p is the specific heat at constant pressure. (For a dilute gas $\zeta=0$.)

At high frequencies, where the attenuation is large, the classical result is no longer accurate. The full Navier–Stokes theory and its extensions to the Burnett and super-Burnett limits have been shown to only qualitatively describe the existing experimental data.[4] Despite this, these results are useful because they are given in closed form and perform reasonably well for frequencies that are not too high ($R>0.5$). For Maxwell molecules, the complex propagation constant $\beta=m/k_0+ik/k_0$ ($k_0=\omega/c$ is the classical wavenumber) is given in terms of R as[4]

$$\beta^4\left(\frac{3}{2}\frac{i}{R}-\frac{10}{3}\frac{1}{R^2}\right)+\beta^2\left(1+\frac{23}{6}\frac{i}{R}\right)+1=0 \tag{5}$$

in the Navier–Stokes theory,

$$\beta^6\left(-\frac{35}{27}\frac{1}{R^4}-\frac{10}{3}\frac{i}{R^3}\right)+\beta^4\left(-\frac{97}{18}\frac{1}{R^2}+\frac{3}{2}\frac{i}{R}\right)+\beta^2\left(1+\frac{23}{6}\frac{i}{R}\right)+1=0 \tag{6}$$

in the Burnett theory and

$$\beta^8\left(\frac{157\times 25}{972}\frac{1}{R^6}-15\frac{i}{R^5}\right)+\beta^6\left(-\frac{805}{54}\frac{1}{R^4}+\frac{67}{24}\frac{i}{R^3}\right)+\beta^4\left(\frac{2275}{216}\frac{i}{R^3}-\frac{97}{18}\frac{1}{R^2}+\frac{3}{2}\frac{i}{R}\right)+\beta^2\left(1+\frac{23}{6}\frac{i}{R}\right)+1=0 \tag{7}$$

in the super-Burnett theory.

Molecular-kinetic calculations have been performed at various levels of approximation and with varying degrees of success in capturing the variation of the attenuation coefficient and sound speed with frequency at the high frequency limit.[3] The Boltzmann equation has been solved approximately by Buckner and Ferziger[14] using the method of elementary solutions and by Sirovich and Thurber[6] using the method of analytic continuation. Both groups considered the linearized model equation by Gross and Jackson.[15] The solution by Sirovich and Thurber has been found to perform well over the whole range for which experimental data exist; their 8-moment and 11-moment results for hard spheres have been transcribed from their paper and are included in Sec. IV for comparison.

IV. SIMULATION RESULTS AND DISCUSSION

We simulated gaseous argon as a hard sphere gas (molecular mass $m_m=6.63\times10^{-26}$ kg, hard sphere diameter $\sigma=3.66\times10^{-10}$ m) at atmospheric conditions ($P=1.013\times10^5$ Pa, $T=273$ K). This choice of species was mainly due to historical and convenience reasons. It has been historically used in a large number of DSMC studies because it provides instant availability to a substantial literature of simulation and experimental results for code validation. The hard sphere model was selected as the intermolecular potential primarily because it is commonly used in the theoretical analysis of high frequency acoustics. More complicated interaction models (e.g., variable hard sphere, variable soft sphere) are often used in DSMC simulations because the temperature dependence of the transport coefficients can be important for accurate computations. However, in our simulations the temperature variations are very small since the wave amplitude was kept small to avoid nonlinear effects.

We ensured that there were 35–40 (on average) molecules per cell, which is substantially more than the number (about 20) empirically determined to be required for accurate solutions.[16,17] Calculations with approximately 100 molecules per cell at selected frequencies yielded identical results. The number of cells was chosen so that the cell linear dimension is less than half of a mean free path. The mean free path for hard spheres is given by $\lambda=m_m/\sqrt{2}\pi\sigma^2\rho$ and $\lambda\approx6.25\times10^{-8}$ m in our simulations. Alexander *et al.*[18] have shown that the transport coefficients deviate from the dilute gas Enskog values as the square of the cell size Δx with the proportionality constant such that for cell sizes of the order of one mean free path, an error of the order of 10% occurs. In our case $\Delta x \approx 0.5\lambda$, so the error is less than 2.5%. We used the results of Alexander *et al.*[18] to correct all our results for the transport coefficients (viscosity and thermal conductivity).

The timestep of the simulation Δt was taken to be significantly smaller than λ/c_o where $c_o=\sqrt{2k_BT/m_m}$ is the most probable velocity. It has been shown[19,20] that the error in the transport coefficients is proportional to the square of the timestep, which for accurate simulations has to be much smaller than λ/c_o. At the highest frequencies the waveform period is significantly smaller than the mean free time and thus a second constraint on the simulation timestep is $\Delta t \approx 2\pi/\omega$. Consequently, the timestep was set to the highest value that would satisfy both $\Delta t<\lambda/(5c_o)$, and $\Delta t<(2\pi/\omega)/60$.

Temperature variations due to dissipation were closely monitored and the mean temperature was found to increase for $R<1$. The maximum temperature increase observed was less than 3%, which leads to a change of less than 2% in the sound speed and transport coefficients given that these vary as $\sqrt{T}$.

Figure 2 shows a comparison between the simulation results and the classical Navier–Stokes theory for $\omega=422$

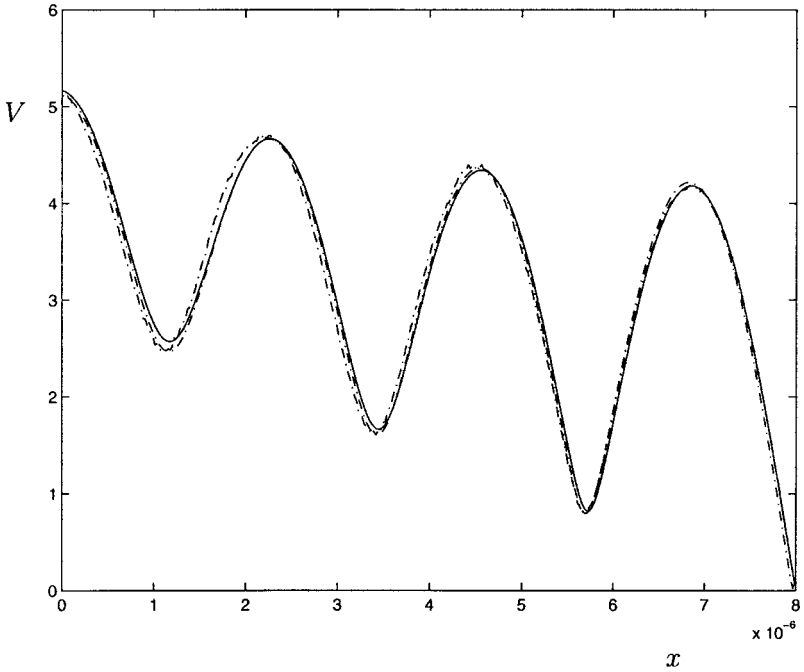

FIG. 2. Velocity amplitude $V(x)=\sqrt{A^2+B^2}$ (in m/s) as a function of distance (in meters) from the driven end for $\omega=422\times10^6$ rad/s ($R\approx20$). The solid line represents the Navier–Stokes prediction, the dash-dotted line represents the simulation result, and the dashed line represents a fit to the simulation results.

$\times10^6$ rad/s. This frequency is low enough that the characteristic time ($2\pi/\omega\sim1.5\times10^{-8}$ s) is much larger than the mean collision time $\tau\approx\lambda/c\sim1.2\times10^{-10}$ s. In this low frequency regime the Navier–Stokes theory is well approximated by the classical theory and successfully captures the physics of wave propagation, as verified by our simulation.

Experimentation at high frequencies is difficult because the strong absorption makes sampling very close to the wall necessary. Greenspan[11] limits his experiments to $R>0.3$ because for $R<0.3$ the ''wave path is shorter than one mean free path'' and sufficient signal only exists at distances less than one mean free path from the input. Measurements closer than one mean free path from the transducer (or from the input reservoir in the simulations) are likely to be skewed by the input's Maxwellian distribution through free molecular flow.[6]

In his discussion Cercignani argues that sufficient collisions take place even at small distances from the input and subsequently the region excluded due to free molecular flow should be much smaller than one mean free path. Additionally he argues that while molecules with high velocities may bias the distribution function at large distances from the input, this is not expected to happen for hard sphere molecules due to the high collision rate associated with high velocity hard spheres. We examine these assertions below.

Our results indicate that the wavelength and attenuation coefficient attain constant values for $x>\lambda$. This is illustrated by considering the same data ($R=0.5$) but restricting the fit to $x>x_{\min}$ with $x_{\min}=\lambda$ in Fig. 3 and $x_{\min}=0.5\lambda$ in Fig. 4. Figure 3 shows that the waveforms are fitted very well by a constant sound speed and attenuation coefficient model for $x>\lambda$; the fit extrapolated in the region $0<x<\lambda$ deteriorates very quickly, indicating that the free molecular flow is still important for $x<\lambda$. Figure 4 shows that the same constant parameters cannot fit the waveform for both $x<\lambda$ and $x>\lambda$.

Figures 5 and 6 summarize our computational results for the sound speed and the attenuation coefficient in the range 52×10^6 rad/s$<\omega<129.8\times10^9$ rad/s. Selected experimental data points from Greenspan,[4] and Meyer and Sessler,[5] as well as the theoretical predictions of the Navier–Stokes, Burnett and super-Burnett theories and the 8- and 11-moment results of Sirovich and Thurber are shown. Several other theories[21–23] (not graphed) are in fair agreement with our sound speed results but predict a smaller absorption coefficient at the higher frequencies ($R<5$).

Unfortunately, for $R<0.25$ the available signal is very weak and the results obtained using $x_{\min}=\lambda$ may be inaccurate. For R 0.5 we also considered $x_{\min}=0.5\lambda$ and the values of m and k thus obtained are denoted by the circled stars in Figs. 5 and 6. Note that for three frequencies (between $R=0.1$ and 0.5) the results from both fits are shown and the variation in the curve fits indicates the sensitivity of the results to the choice of $x_{\min}$. As can be seen from Figs. 3 and 4, for $x<\lambda$, that is in the region where free molecular flow is significant, the wavelength is shorter and the attenuation coefficient lower. This is very important in connection with the reported experimental results for $R<0.25$.

We should also reemphasize that for $R<4$ larger initial amplitudes were gradually introduced due to the appreciable attenuation. The wave amplitude at the reservoir was increased up to $v_o/c=0.15$ to ensure that sufficient signal existed for $x>x_{\min}$ (curve fit region); however, care was taken to ensure that $v_o\exp(-mx_{\min})/c<0.025$.

In summary, we find that our simulation results are consistent with the experimental data, and verify the observations of Cercignani[3] that the classical Navier–Stokes description fails for $R<10$, and that none of the proposed theories can capture the variation of both sound speed

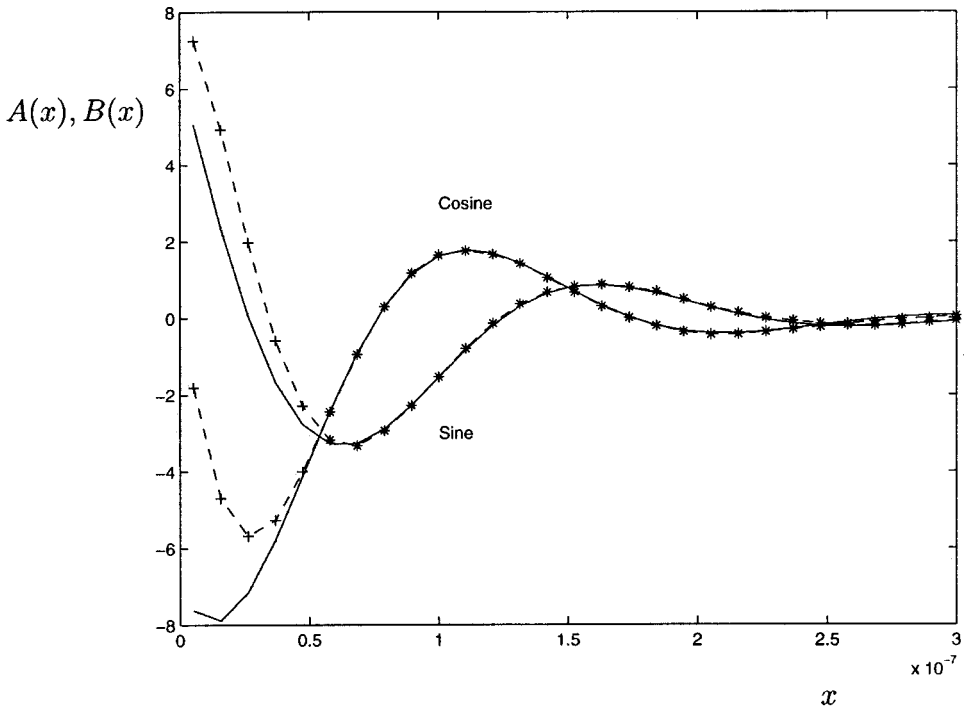

FIG. 3. Cosine and sine components, $A(x)$ and $B(x)$, of the velocity amplitude (in m/s) for $\omega=16.2\times10^9$ rad/s ($R=0.5$). The waveforms are fitted for $x>x_{\min}=\lambda$ to extract a sound speed of 464.1 m/s and an attenuation coefficient of 1.42×10^7 m^{-1} at this frequency. The stars denote simulation data used for the fit (solid line) and crosses denote simulation data not included in the fit.

and attenuation coefficient over the whole frequency range. Our results offer significantly less scatter compared to the experimental data, which is essential for the development of an accurate theory valid over the whole frequency range.

V. CONCLUDING REMARKS

In this article we consider the acoustic properties of a single species, dilute gas of hard sphere particles for small amplitude oscillations. This study demonstrates the usefulness of the simulation technique; extensions to more complex problems directly follow. For example, the sound speed and absorption are modified by thermal relaxation effects,[2] such as vibrational and rotational degrees of freedom, chemical reactions, etc. Interesting nonhydrodynamic effects in binary mixtures (e.g., ''fast sound''[24,25]) are known to occur at high frequencies. Nonlinear effects become comparable to viscous dissipation at amplitudes a few times larger than those considered here. Finally, the consistent Boltzmann algorithm[26] can be employed to simulate nondilute systems.

Our DSMC technique uses a thermal reservoir with an

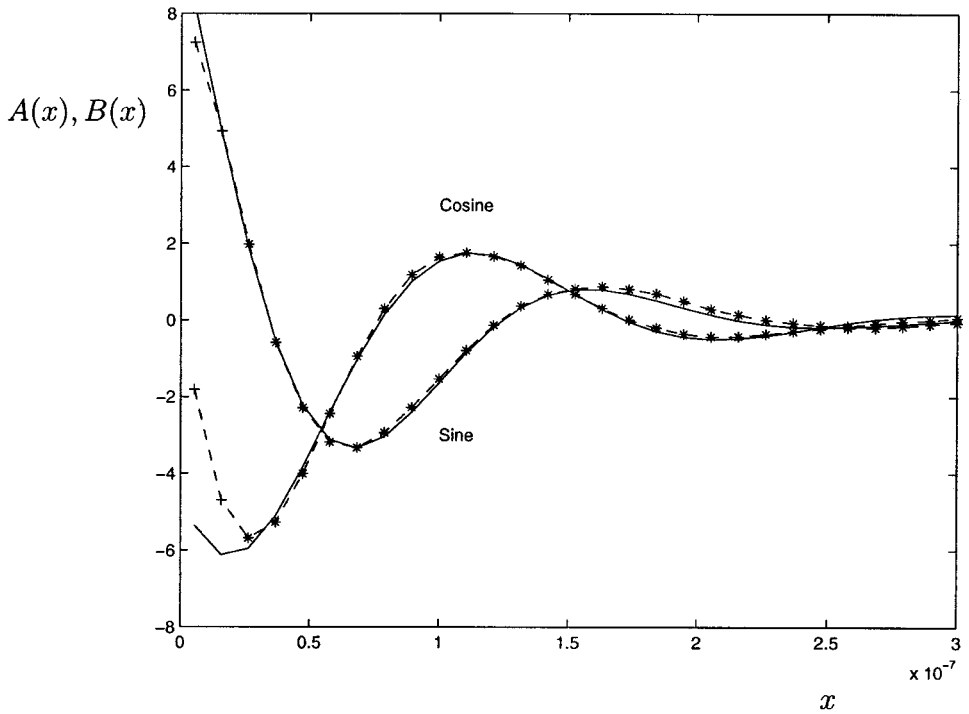

FIG. 4. Cosine and sine components, $A(x)$ and $B(x)$, of the velocity amplitude (in m/s) for $\omega=16.2\times10^9$ rad/s ($R=0.5$). The waveforms are fitted for $x>x_{\min}=0.5\lambda$ giving a sound speed of 515.7 m/s and an attenuation coefficient of 1.45×10^7 m^{-1}. The stars denote simulation data used for the fit (solid line) and crosses denote simulation data not included in the fit.

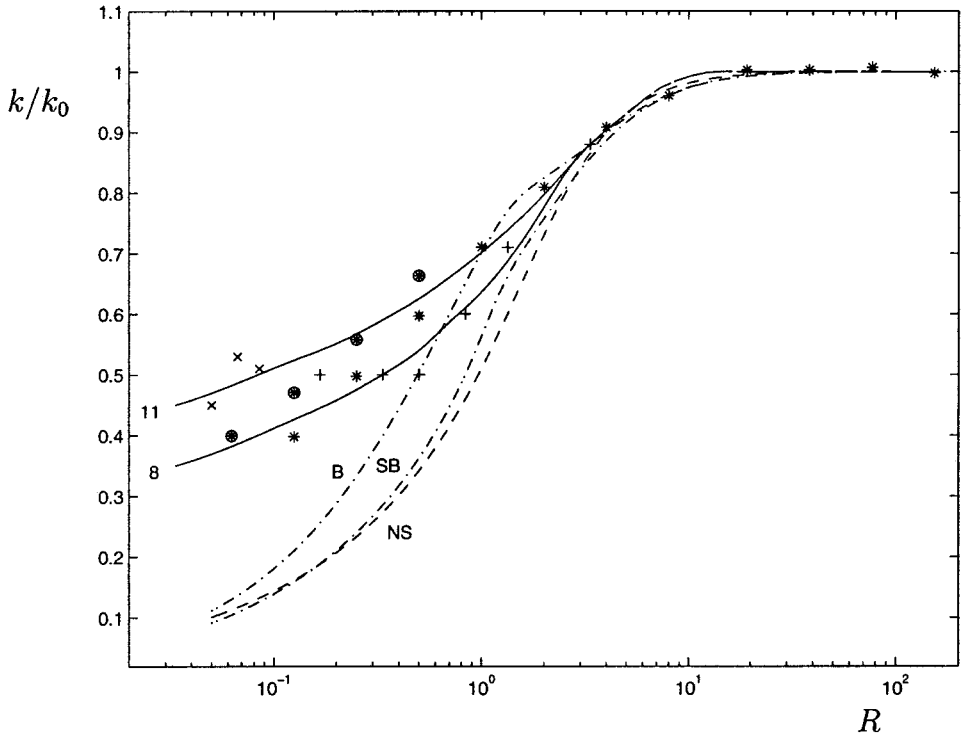

FIG. 5. Scaled inverse sound speed vs scaled inverse frequency. The solid lines represent the 8 and 11 moment solutions, the dashed line represents the Navier–Stokes (NS) prediction, the dash-dotted lines represent the Burnett (B) and super-Burnett (SB) solutions, the crosses represent experimental data ($\times$ for Meyer and Sessler, and $+$ for Greenspan), and the stars (*) are the DSMC simulation results. Plain stars denote sampling for $x_{\min} = \lambda$ and circled stars denote sampling for $x_{\min} = 0.5\lambda$.

oscillating mean velocity at the domain inlet ($x=0$), to produce the input sound wave. Instead of generating the particles with a Maxwell–Boltzmann distribution, the Chapman–Enskog distribution[27] may be used to approximate bulk conditions, possibly minimizing the inhomogeneity associated with free molecule effects. Alternatively, an oscillating solid wall (i.e., a transducer piston) can be used as the acoustic source. This surface should be thermal rather than specular, otherwise there would be no way to remove the heat generated by viscous dissipation. Such a wall in conjunction with DSMC collision models that capture real-gas non-hard-sphere interactions[8] is expected to be a better model of a typical experimental setup. However, we expect that these different methods of simulating the input acoustic source will have little effect on the sound speed and attenuation prediction presented here since our curve fits excluded the region nearest to the excitation point. However, the phase shift in the free molecular regime near the excitation point

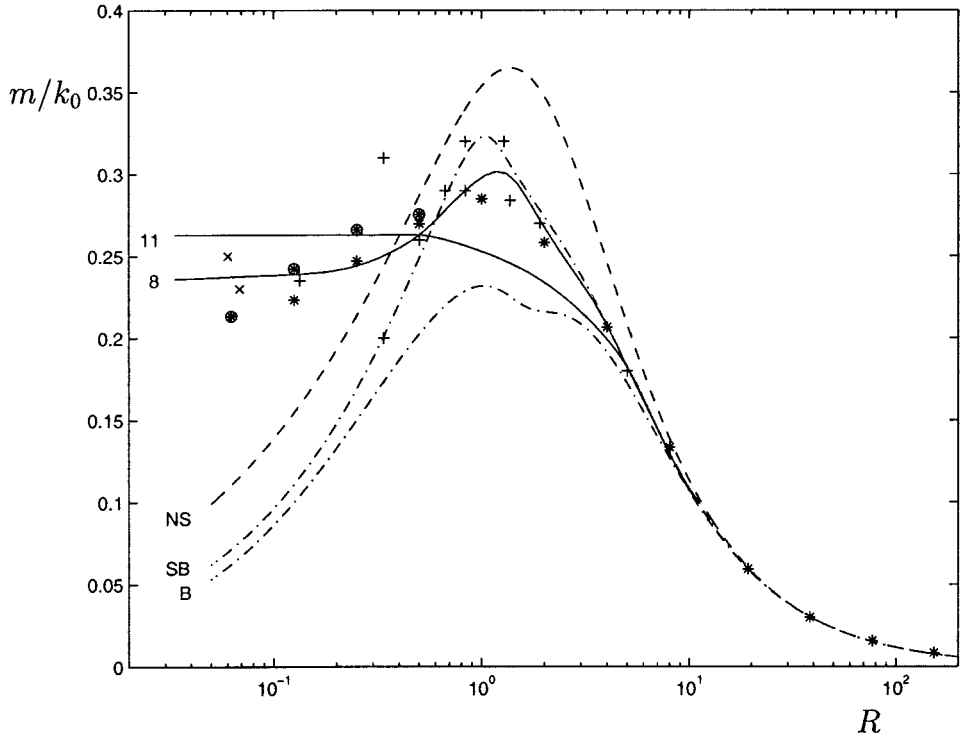

FIG. 6. Scaled absorption coefficient vs scaled inverse frequency. The solid lines represent the 8 and 11 moment solutions, the dashed line represents the Navier–Stokes (NS) prediction, the dash-dotted lines represent the Burnett (B) and super-Burnett (SB) solutions, the crosses represent experimental data ($\times$ for Meyer and Sessler, and $+$ for Greenspan), and the stars (*) are the DSMC simulation results. Plain stars denote sampling for $x_{\min} = \lambda$ and circled stars denote sampling for $x_{\min} = 0.5\lambda$.

may be sensitive to the various input boundary conditions and an analysis of this effect would be of interest. Finally, by replacing the specular surface at $x=L$ with a stationary, constant temperature wall, the reflection phase shift of a solid[2] can be computed.

ACKNOWLEDGMENTS

The authors wish to thank B. Alder and M. Malek-Mansour for helpful discussions. This work was performed while one author (N.H.) was visiting the Center for Applied Scientific Computing (CASC) at Lawrence Livermore National Laboratory. The authors would like to thank Xabier Garaizar for the hospitality and for making this work possible through the computer resources made available to the authors, and Dr. Kyran Mish, Director, Center for Computational Engineering, Lawrence Livermore National Laboratory, for financial support (U.S. Department of Energy, W-7405-ENG-48). This work was also supported in part by a grant from the European Commission DG12 (PSS*1045).

[1] J. W. S. Rayleigh, *The Theory of Sound* (Macmillan, New York, 1896), Vol. 2.
[2] L. D. Landau and E. M. Lifshitz, *Fluid Mechanics* (Pergamon, New York, 1989).
[3] C. Cercignani, *The Boltzmann Equation and its Applications* (Springer-Verlag, New York, 1988).
[4] M. Greenspan, ''Propagation of sound in five monoatomic gases,'' J. Acoust. Soc. Am. **28**, 644 (1956).
[5] E. Meyer and G. Sessler, ''Schallausbreitung in Gasen bei hohen Frequenzen und sehr niedrigen Drucken,'' Z. Phys. **149**, 15 (1957).
[6] L. Sirovich and J. K. Thurber, ''Propagation of forced sound waves in rarefied gasdynamics,'' J. Acoust. Soc. Am. **37**, 329 (1965).
[7] F. J. Alexander and A. L. Garcia, ''The direct simulation Monte Carlo method,'' Comput. Phys. **11**, 588 (1997).
[8] G. A. Bird, *Molecular Gas Dynamics and the Direct Simulation of Gas Flows* (Clarendon, Oxford, 1994).
[9] W. Wagner, ''A convergence proof for Bird's direct simulation Monte Carlo method for the Boltzmann equation,'' J. Stat. Phys. **66**, 1011 (1992).
[10] E. S. Oran, C. K. Oh, and B. Z. Cybyk, ''Direct simulation Monte Carlo: Recent advances and applications,'' Annu. Rev. Fluid Mech. **30**, 403 (1998).
[11] M. Greenspan and M. C. Thompson, Jr., ''An eleven megacycle interferometer for low pressure gases,'' J. Acoust. Soc. Am. **25**, 92 (1953).
[12] P. M. Morse and K. U. Ingard, *Theoretical Acoustics* (McGraw–Hill, New York, 1968).
[13] W. H. Press, S. A. Teukolsky, W. T. Vetterling, and B. P. Flannery, *Numerical Recipes in C*, 2nd ed. (Cambridge University Press, Cambridge, 1992).
[14] J. Buckner and J. Ferziger, ''Linearized boundary value problem for a gas and sound propagation,'' Phys. Fluids **9**, 2315 (1966).
[15] E. P. Gross and E. A. Jackson, ''Kinetic models and the linearized Boltzmann equation,'' Phys. Fluids **2**, 432 (1959).
[16] M. Fallavollita, D. Baganoff, and J. McDonald, ''Reduction of simulation cost and error for particle simulations of rarefied flows,'' J. Comput. Phys. **109**, 30 (1993).
[17] G. Chen and I. Boyd, ''Statistical error analysis for the direct simulation Monte Carlo technique,'' J. Comput. Phys. **126**, 434 (1996).
[18] F. Alexander, A. Garcia, and B. Alder, ''Cell size dependence of transport coefficients in stochastic particle algorithms,'' Phys. Fluids **10**, 1540 (1998); erratum, **12**, 731 (2000).
[19] N. G. Hadjiconstantinou, ''Analysis of discretization in the direct simulation Monte Carlo,'' Phys. Fluids **12**, 2634 (2000).
[20] A. Garcia and W. Wagner, ''Time step truncation error in direct simulation Monte Carlo,'' Phys. Fluids **12**, 2621 (2000).
[21] L. C. Woods and H. Troughton, ''Transport processes in dilute gases over the whole range of Knudsen numbers; Part 2, Ultrasonic sound waves,'' J. Fluid Mech. **100**, 321 (1980).
[22] A. M. Anile and S. Pluchino, ''Linear wave modes in nonlocal fluid dynamics,'' Meccanica **19**, 104 (1984).
[23] G. Lebon and A. Cloot, ''Propagation of ultrasonic sound waves in dissipative dilute gases and extended irreversible thermodynamics,'' Wave Motion **11**, 23 (1989).
[24] R. Huck and E. Johnson, ''Possibility of double sound propagation in disparate-mass gas mixtures,'' Phys. Rev. Lett. **44**, 142 (1980).
[25] W. Montfrooij, P. Westerhuijs, V. de Haan, and I. de Schepper, ''Fast sound in a helium–neon mixture determined by neutron scattering,'' Phys. Rev. Lett. **63**, 544 (1989).
[26] F. Alexander, A. Garcia, and B. Alder, ''A consistent Boltzmann algorithm,'' Phys. Rev. Lett. **74**, 5212 (1995).
[27] A. Garcia and B. Alder, ''Generation of the Chapman–Enskog distribution,'' J. Comput. Phys. **140**, 66 (1998).